

# Type Classification of Sudden Stratospheric Warming Based on Pre- and Postwarming Periods

HYESUN CHOI

*School of Earth and Environmental Sciences, Seoul National University, Seoul, and Korea Polar Research Institute, Incheon, South Korea*

BAEK-MIN KIM<sup>a</sup>

*Korea Polar Research Institute, Incheon, Korea*

WOOKAP CHOI

*School of Earth and Environmental Sciences, Seoul National University, Seoul, South Korea*

(Manuscript received 12 April 2018, in final form 22 January 2019)

## ABSTRACT

In existing literature, sudden stratospheric warming (SSW) events have been typically defined as displacement or split types. Detailed reexamination of SSW evolution has revealed that an SSW event often alters its type before and after the central day of the warming event. On the basis of this observation, we objectively define three types of SSW using wave amplitude: displacement–displacement (DD) type, displacement–split (DS) type, and split–split (SS) type. The geopotential height (GPH) amplitude of zonal wavenumbers 1 and 2 averaged over 55°–65°N at 10 hPa was used as a criterion for the classification. If the amplitude of zonal wavenumber 1 is larger (smaller) than that of wavenumber 2 before and after the central day of SSW, the event is regarded as a DD (SS) type. If the amplitude of zonal wavenumber 1 is larger than that of wavenumber 2 before the central day but is smaller after that day, the event is regarded as a DS type. The above classification algorithm has been applied to both reanalysis data and model results. We observe that conventional split-type SSW events identified by previous studies can be categorized as either DS- or SS-type events, each type of which exhibits different evolution characteristics. In particular, they are distinctively different during the prewarming period. In the SS type, the characteristics of the conventional split type are more obvious, and the features that differ from those of the DD type are the most robust. The model results generally resemble the reanalysis data, particularly in the DD cases.

## 1. Introduction

Since it was first observed in 1952, sudden stratospheric warming (SSW) has been a stratospheric climate variability of major interest in the Northern Hemisphere (NH) winter season. This phenomenon is characterized by a rapid increase in polar stratospheric temperature and an abrupt decrease in circumpolar zonal wind; various methods of defining SSW have been detailed by [Butler et al. \(2015\)](#). The change in zonal flow is accompanied by deformation in the shape of the polar vortex.

The SSW type can be distinguished depending on the vortex shape. More than half of SSW events are categorized as displacement type because the center of polar vortex shifts toward lower latitudes. The other SSW event type is known as split type because the polar vortex splits into two vortices of similar size and strength. This displacement and splitting of the polar vortex are regarded as wave-1 and wave-2 types, respectively.

[Yoden et al. \(1999\)](#) used the relative strength of stratospheric planetary waves to classify the SSW type. [Bancalá et al. \(2012\)](#) and [Barriopedro and Calvo \(2014\)](#), hereafter BC14) also used dominant waves to classify SSW. [Charlton and Polvani \(2007\)](#), hereafter CP07) used absolute vorticity on the pressure surface to objectively classify the type; this method was also used by [Cohen and Jones \(2011\)](#), hereafter CJ11). [Mitchell et al. \(2013\)](#)

<sup>a</sup> Current affiliation: Department of Environmental Atmospheric Sciences, Pukyong National University, Pusan, South Korea.

Corresponding author: Wookap Choi, wchoi@snu.ac.kr

suggested a classification algorithm by using the area, shape, and location of the vortex. Lawrence and Manney (2018) introduced computer vision techniques to analyze the geometry of the Arctic polar vortex and showed the applicability of this method as an analysis tool.

A significant factor in determining the type appears to be the time at which the SSW is characterized. Several studies, including Yoden et al. (1999) and Bancalá et al. (2012), focused on the wave evolution features exhibited during the prewarming phase, whereas CP07 considered vortex separation during the period comprising both the prewarming and postwarming phases to classify the type.

A comparison between the Bancalá et al. (2012) classification results and those of CP07 shows that all wave-2 types correspond to the split type but not all wave-1 types match the displacement type. This is because some wave-1 types lead to a split event during the postwarming phase (Bancalá et al. 2012). This type has been referred to as hybrid type (O'Neill 2003), mixed type (Mitchell et al. 2013), wave-1 amplification-related splitting event (BC14), and wave-1 splitting event (Bancalá et al. 2012). Because the mixed type is influenced by timing, which is considered to characterize the SSW type, the group to which it belongs may vary among studies. Nevertheless, the impact of the mixed type on composite analysis studies, which is used to identify general features based on SSW type, has not been examined in detail.

In the process of analyzing the data to identify the dynamical features of SSW events based on the traditional classification of the two types, we found two distinctive groups of SSW among the split-type events. Thus, in contrast to the previous studies, we intend to classify SSW into three types considering its evolution before and after the central day of the warming event. To accomplish this, a simple objective algorithm that considers wave amplitude is used. Different characteristics, depending on the SSW type, are identified by using reanalysis data and model results. As discussed subsequently, the differences among these three types are more robust than those reported between the traditional displacement and split types. Therefore, considering these three types are distinctively different from each other, it is more appropriate to classify SSWs into three types rather than two types to achieve a better understanding of SSW events.

In section 2, the reanalysis data and the model used for simulation are described. In section 3, we suggest a method for classifying SSW events into three types, and we discuss the different features depending on the type using the reanalysis data. The model results are shown in section 4, and a summary and discussion are presented in section 5.

## 2. Data and model

### a. Data

The two datasets used for this analysis are the Modern-Era Retrospective Analysis for Research and Applications (MERRA) assimilated data (inst3\_3d\_asm\_Cp; Rienecker et al. 2011) and National Centers for Environmental Prediction–National Center for Atmospheric Research (NCEP–NCAR) reanalysis data (Kalnay et al. 1996). From the MERRA data, zonal and meridional winds, air temperature, and geopotential height (GPH) were obtained with a horizontal resolution of  $1.25^\circ$  latitude  $\times$   $1.25^\circ$  longitude at 42 pressure levels from 1000 to 0.1 hPa from 1 January 1979 to 31 December 2014. From the NCEP–NCAR data, zonal and meridional winds, air temperature, and GPH are presented with a horizontal resolution of  $2.5^\circ$  latitude  $\times$   $2.5^\circ$  longitude at 17 pressure levels from 1000 to 10 hPa and sea level pressure from 1 January 1957 to 31 December 2014.

The climatological values were calculated daily from each variable based on the period 1979–2011 for MERRA and 1981–2010 for NCEP–NCAR and were smoothed by a 31-day running mean. In this study, all anomaly fields are defined by perturbations from these 31-day running mean climatological values.

### b. Model

For model simulations, the Whole Atmosphere Community Climate Model (WACCM) was used. WACCM is the atmospheric component of the Community Earth System Model (CESM1.0.6) and includes all physical parameterizations of Community Atmospheric Model, version 4 (Neale et al. 2012). WACCM has a horizontal resolution of  $1.9^\circ$  latitude  $\times$   $2.5^\circ$  longitude at 66 hybrid pressure-sigma levels from the surface to 140 km in terms of log-pressure altitude with variable vertical resolution. The vertical coordinate was converted into a pressure coordinate with 43 levels from 1000 to 0.0001 hPa (about 112.8 km) before analysis. For the lower boundary conditions, sea surface temperature, and sea ice data were obtained from the monthly Hadley Centre Sea Ice and Sea Surface Temperature dataset (Rayner et al. 2003). For chemical conditions, the configurations of perpetual AD 2000 and specified chemistry (SC) were used. The SC–WACCM is known to reduce the computational cost to approximately one-half that of WACCM (Smith et al. 2014). No significant differences were noted in the simulation of the surface, tropospheric, and stratospheric climate compared with WACCM values under pre-industrial conditions (Smith et al. 2014).

This model has been used in previous studies and has produced the major SSW events in the NH at frequencies comparable to those revealed by observations

(Richter et al. 2010; Limpasuvan et al. 2012; de la Torre et al. 2012; Marsh et al. 2013).

In the WACCM simulations, focus is placed on the internal dynamics of the stratosphere under the climatological boundary conditions. The model excluded interannual variability originating from the troposphere, such as El Niño–Southern Oscillation (ENSO) and sea ice melting. The monthly sea surface temperature and sea ice data from 1981 to 2010 were averaged, and their annually varying climatological values were prescribed repeatedly every year in the model. The model has been run for 211 years; 200 boreal winters (October–March) from the last 201 years were analyzed. In all analyses, a Student's *t* test was applied for statistical significance testing.

### 3. Classification of SSW type

To classify the major SSW events in this study, we used a common definition based on the zonal-mean zonal wind at 10 hPa and 60°N during the boreal winter season (1 October–31 March). A zonal wind reversal from westerly to easterly indicates a major SSW event; the first day of the wind reversal is defined as the central day of the SSW. To distinguish SSW from stratospheric final warming, the central day should appear at least 10 days before the end of March, and the westerly zonal wind should recover before the end of March. On this basis, 37 and 25 major SSW events were identified from the NCEP–NCAR reanalysis from 1957 to 2014 and from the MERRA data from 1979 to 2014, respectively. The frequency of the SSW occurrence per year was 0.65 for NCEP–NCAR and 0.7 for MERRA, which is similar to that found in CP07 (0.62).

#### a. Classification algorithm

Classification of SSW type requires consideration of the time evolution of the vortex shape. Waugh (1997) represented polar vortices by using elliptic shapes. A widely accepted method suggested by CP07 carefully considers the two-dimensional development of SSW. Although their sophisticated classification method has been continually used and developed (Cohen and Jones 2011; Mitchell et al. 2013; Lawrence and Manney 2018), it requires complex calculations. To avoid these computational complexities, we used simple harmonic analysis to obtain results very similar to those from previous studies, such as CP07. Because the SSW types of displacement and split show dominant patterns of wave 1 and wave 2, respectively, we began the classification based on the amplitude of zonal waves 1 and 2 by using harmonic analysis. The process is described as follows:

- 1) For an individual SSW event, the daily GPH averaged over 55°–65°N at 10 hPa was decomposed by harmonic analysis to obtain the amplitude for zonal waves 1 and 2. We examined the frequency of each type for the five latitude belts of 10° width, shifting 5° from 45°–55° to 65°–75°N. The band of latitude 55°–65°N was selected because the classification results based on this latitude band are the closest to those reported by CP07. The sensitivity of the SSW-type classification to these five latitude bands is discussed in section 3c.
- 2) This analysis was conducted for a period of 21 days, from 10 days before the central day to 10 days afterward. We tested the sensitivity to the period of analysis by changing the pre- and postevent periods from 10 to 15 days. However, the analysis period did not appear to be crucial for determining the type, as noted in section 3c. Throughout the 21 days of analysis, if the amplitude of wave 2 was larger than that of wave 1 on any day, the event was regarded as a wave-2 type; otherwise, it was regarded as a wave-1 type. Although the names “wave 1” and “wave 2” were used temporarily for convenience, these two types are, in fact, very similar to the displacement and split types, respectively. Their similarities are shown in Table 1.

The amplitudes of waves 1 and 2 were obtained through the process described above by using MERRA data. Their ratios are shown in Fig. 1 for SSW events from 14 days before the central day (0) to 14 days afterward. For the 13 wave-1-type events (Fig. 1a), from day –10 to day 10, the ratios exhibited small variations and imply that the amplitude of wave 2 was relatively small. On the contrary, for the 12 wave-2 types (Fig. 1b), the amplitudes were sometimes significantly larger than those of wave 1. The most prominent example is the 24 January 2009 SSW event, represented by the dashed line in Fig. 1b. Moreover, for the wave-2 type shown in Fig. 1b, two peaks occurred in the composited ratio. These double peaks imply that some of the SSW events had a large wave 2 either before or after the central day or both.

#### b. Objective definition of the displacement–split type

To determine whether all of the SSW events in Fig. 1b had similar characteristic features, the wave-2 types were separated into two groups, as shown in Fig. 2. Figure 2a shows the cases in which a ratio larger than the threshold value of 1 was observed between day 0 and day +10 (i.e., only after the central day). In these 7 cases out of 12, behavior similar to that shown in Fig. 1a, before the central day, is presented in Fig. 2a. Figure 2b

TABLE 1. SSW events identified from the NCEP–NCAR (columns 2 and 3) and MERRA (columns 4 and 5) datasets and from CJ11 (columns 6 and 7) and CP07 (column 8). Letters in italics indicate SSWs found in only one dataset. Bold letters denote different classification among the studies.

No.	NCEP–NCAR		MERRA		CJ11		CP07
	Central date	Type	Central date	Type	Central date	Type	Type subjective
1	30 Jan 1958	SS			30 Jan 1958	S	S
2	30 Nov 1958	DD			30 Nov 1958	D	D
3	16 Jan 1960	DD			16 Jan 1960	D	D
4	—	—			<i>23 Mar 1965</i>	S	S
5	8 Dec 1965	DD			8 Dec 1965	D	D
6	24 Feb 1966	DS			24 Feb 1966	S	S
7	—	—			<i>8 Jan 1968</i>	S	S
8	27 Nov 1968	DD			27 Nov 1968	D	D
9	14 Mar 1969	DD			13 Mar 1969	D	D
10	2 Jan 1970	DD			2 Jan 1970	D	D
11	17 Jan 1971	DS			17 Jan 1971	S	S
12	20 Mar 1971	DD			20 Mar 1971	D	D
13	2 Feb 1973	DS			2 Feb 1973	S	S
14	<i>13 Mar 1974</i>	<i>DD</i>			—		—
15	<i>15 Mar 1975</i>	<i>DD</i>			—		—
16	<i>12 Mar 1978</i>	<i>DS</i>			—		—
17	22 Feb 1979	SS			22 Feb 1979	S	S
18	29 Feb 1980	DD	29 Feb 1980	DD	29 Feb 1980	D	D
19			<i>4 Mar 1981</i>	<i>DS</i>			
20	4 Dec 1981	DD	4 Dec 1981	DD	4 Dec 1981	D	D
21	24 Feb 1984	DD	24 Feb 1984	DD	24 Feb 1984	D	D
22	2 Jan 1985	SS	1 Jan 1985	SS	2 Jan 1985	S	S
23	23 Jan 1987	DD	23 Jan 1987	DD	23 Jan 1987	D	D
24	8 Dec 1987	DS	8 Dec 1987	DS	8 Dec 1987	S	S
25	14 Mar 1988	SS	14 Mar 1988	SS	14 Mar 1988	S	S
26	22 Feb 1989	SS	21 Feb 1989	SS	22 Feb 1989	S	S
27			<i>5 Feb 1995</i>	<i>DD</i>			
28	15 Dec 1998	<b>DS</b>	15 Dec 1998	<b>DS</b>	15 Dec 1998	<b>D</b>	<b>D</b>
29	25 Feb 1999	<b>DD</b>	26 Feb 1999	<b>DD</b>	25 Feb 1999	<b>S</b>	<b>S</b>
30	20 Mar 2000	DD	20 Mar 2000	DD	20 Mar 2000	D	D
31					<i>16 Dec 2000</i>	D	
32	11 Feb 2001	DS	11 Feb 2001	DS	11 Feb 2001	S	S
33	2 Jan 2002	DD	30 Dec 2001	DD	2 Jan 2002	D	D
34			<i>17 Feb 2002</i>	<i>DD</i>			
35	18 Jan 2003	DS	18 Jan 2003	DS	18 Jan 2003	S	
36	7 Jan 2004	DD	4 Jan 2004	DD	7 Jan 2004	D	
37	12 Mar 2005	DD	12 Mar 2005	DD			
38	21 Jan 2006	<b>DD</b>	21 Jan 2006	<b>DD</b>	21 Jan 2006	<b>S</b>	
39	24 Feb 2007	<b>SD</b>	24 Feb 2007	<b>SD</b>	24 Feb 2007	<b>D</b>	
40	22 Feb 2008	DD	22 Feb 2008	DD	22 Feb 2008	D	
41	24 Jan 2009	SS	24 Jan 2009	SS	24 Jan 2009	S	
42	9 Feb 2010	DS	9 Feb 2010	DS	9 Feb 2010	S	
43	7 Jan 2013	DS	6 Jan 2013	DS			

shows that five SSW events had a ratio larger than the threshold value of 1 before the central day (from  $-10$  to  $-1$ ). Based on the temporal evolution of the ratio during the prewarming and postwarming phases given in Fig. 2, we classified the SSW events in Fig. 2a as displacement–split (DS) type and those in Fig. 2b as split–split (SS) type. Although the DS type is explicitly defined here objectively, it has been described previously by other names, as discussed in the introduction. In the DS type, the composited ratio gradually increases

after the central day and exceeds the threshold value of 1 after about 5 days. The increase in the ratio during the SSW events is related to the fact that the wave-1 amplitude decreases more than the wave-2 amplitude increases (not shown). On the contrary, the large ratio in the SS type is attributed to the development of wave 2. Among the SS types (Fig. 2b), a single SSW event was noted in which the ratio was below 1 for the postwarming phase (from day +1 to +10). This event could have been classified as split–displacement (SD) type.

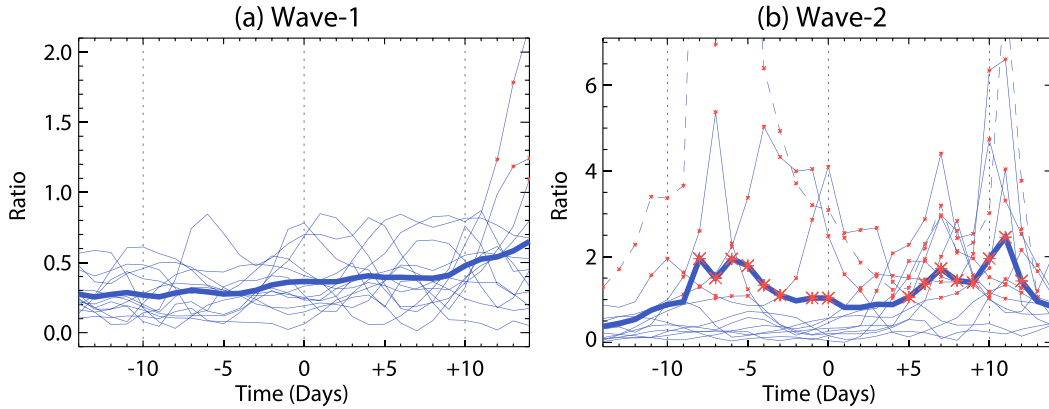


FIG. 1. Temporal evolution of the amplitude ratio of wave 2 to wave 1. Thin lines represent individual SSW events, and the thick line shows their composite mean. Ratios larger than 1.0 are shown with a red asterisk. (a) The 13 wave-1 type SSW events; (b) the 12 wave-2 type SSW events. The dashed line in (b) corresponds to an SSW event occurring on 24 Jan 2009 with maximum ratios of 14.9 on day  $-8$  and 8.3 on day  $+11$ . It should be noted that the range of the vertical axis is different between (a) and (b).

However, because it was observed only once in both the MERRA and NCEP–NCAR data (24 February 2007), this type will not be discussed further.

In the name of each type, the first and second characters represent both the dominant wavenumber and the shape of the polar vortex before and after the central day. The D represents wave 1 and vortex displacement, and S denotes the wave 2 and vortex split. As shown in Fig. 1a, wave 1 persisted both before and after the central day and was classified as displacement–displacement (DD) type by applying the same naming scheme. Hereafter, the above three types will be used for classification.

To show the validity of separating the wave-2 type into DS and SS, a typical SSW event was selected from each type to reveal the evolution of the synoptic structure depending on the type. Figure 3 shows the temporal evolution of the GPH at 10 hPa for the three

different SSW types. The SSW events of 22 February 2008, 8 December 1987, and 1 January 1985, were selected to represent DD, DS, and SS type, respectively. As shown in Fig. 2b, the most prominent SS event was the SSW occurring on 24 January 2009. This case exhibited exceptional development of wave 2 compared with the other SS events and has been extensively studied (Manney et al. 2009; Harada et al. 2010; Ayarzagüena et al. 2011; Coy et al. 2011; Albers and Birner 2014; Kodera et al. 2015, 2016; Wang et al. 2016). However, because this case can be considered as an exception to the typical SS type, we selected a different SSW event, occurring in 1985, to show a more typical example.

The DD-type SSW event shown in Fig. 3a is characterized by a single displaced polar vortex shaded in blue and a wave-1 pattern throughout the SSW period. The

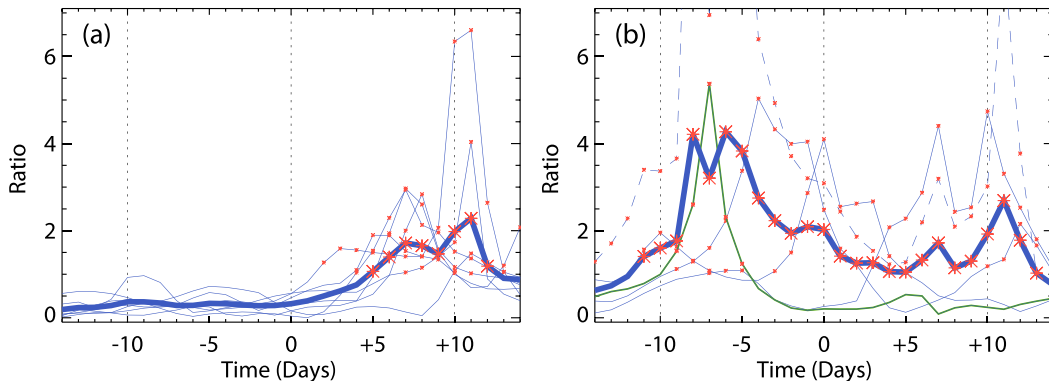


FIG. 2. As in Fig. 1, but for (a) seven DS types and (b) five SS types. The dashed line and the green line in (b) correspond to SSW events occurring on 24 Jan 2009 and on 24 Feb 2007, respectively. DS and SS types are defined in the manuscript.

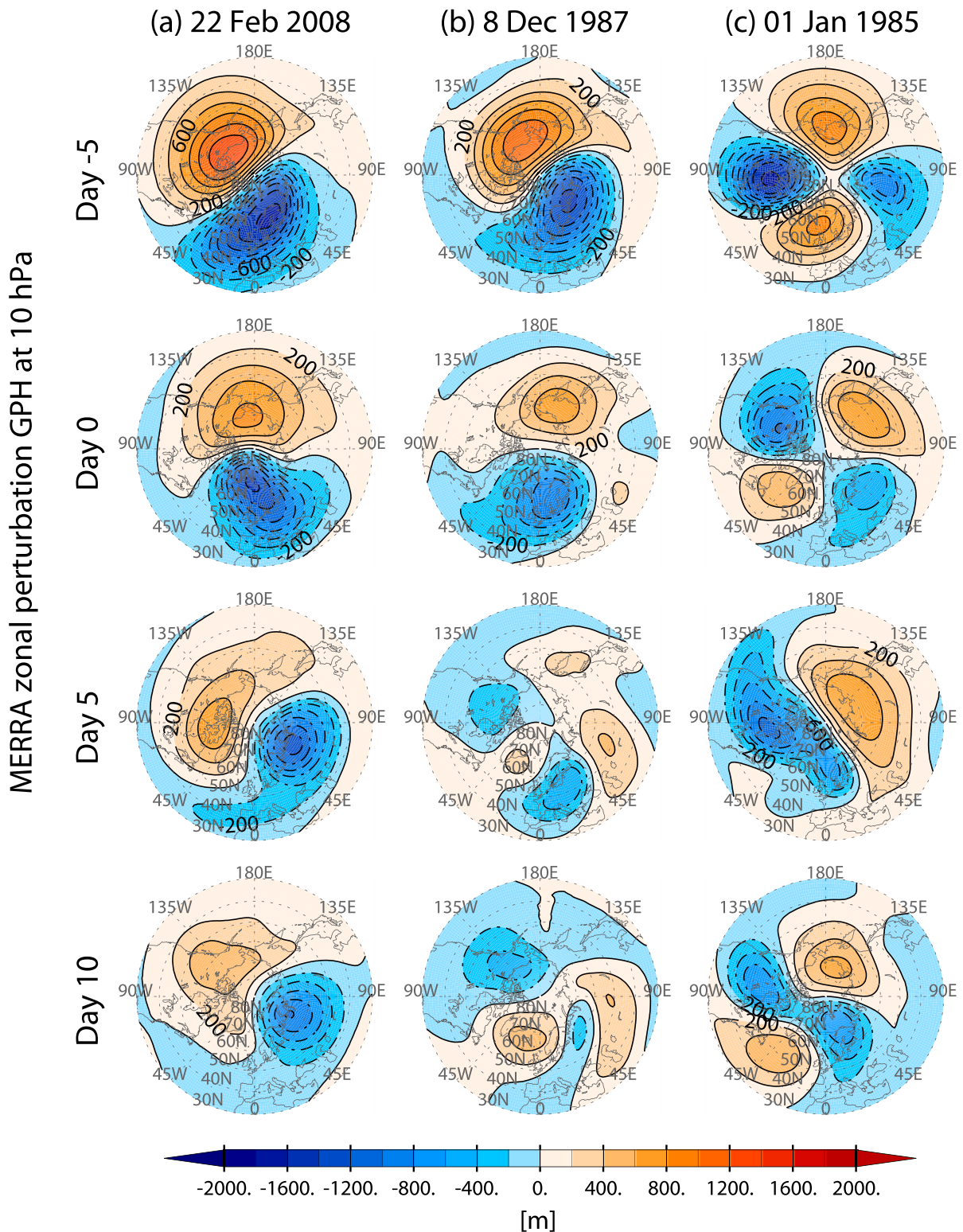


FIG. 3. Zonal perturbation GPH at 10 hPa with a 5-day interval based on MERRA data. (a) DD-type warming on 22 Feb 2008; (b) DS-type warming on 8 Dec 1987; (c) SS-type warming on 1 Jan 1985. The contour interval is 200 m.

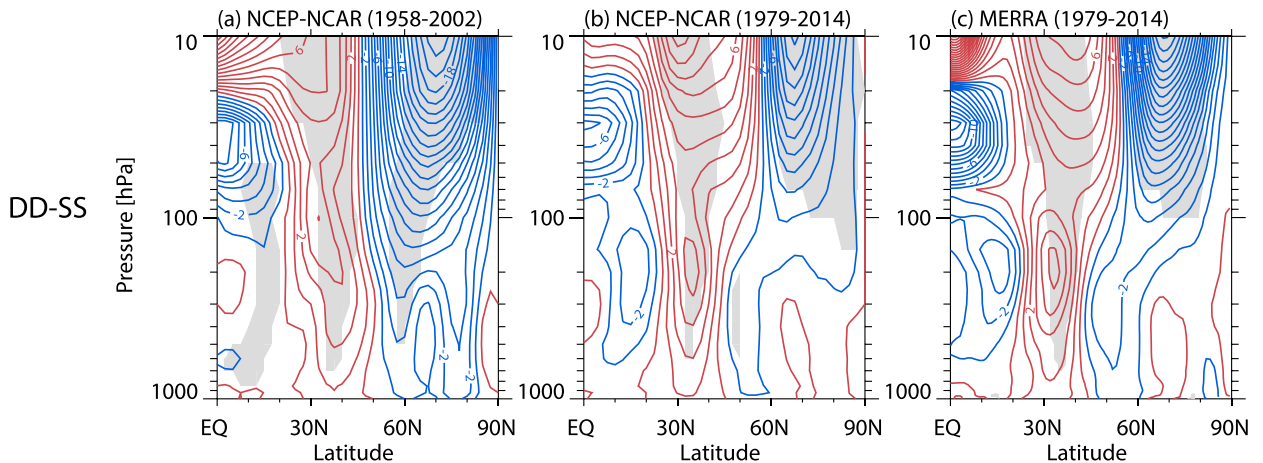


FIG. 4. Differences in zonal-mean zonal wind anomalies averaged from days  $-20$  to  $-5$  between DD and SS types for (a) 1958–2002 based on NCEP–NCAR data, (b) 1979–2014 based on NCEP–NCAR data, and (c) 1979–2014 based on MERRA data. The numbers of DD- and SS-type events are 16 and 5 in (a), 11 and 5 in (b), and 13 and 5 in (c), respectively. The contour interval is  $1.0 \text{ m s}^{-1}$ . The blue and red contours indicate negative and positive differences, respectively. Gray shading indicates the region of statistical significance at the 90% confidence level.

DS type in Fig. 3b shows a pattern similar to the DD type before the central day, with wave-1 characteristics and a displaced vortex. During the postwarming period, however, the vortex moved westward and split into a wave-2 pattern. In the SS type shown in Fig. 3c, the polar vortex shows a wave-2 pattern throughout the SSW period. As expected from the name of each type, DD and DS types share similarities during the prewarming period, and the DS and SS types resemble each other during the postwarming periods. It can be confirmed that the number of the wave between the dominant planetary waves 1 and 2 is consistent with the shape of the polar vortex and that the DS type should be separated from the SS type. An exception was observed on day 5 in Fig. 3c in which the structure of the SS type was rather similar to a wave-1 pattern. This occurred because the wave-2 activity weakened temporarily with the minimum on day 5.

To show a clear distinction between the SS and DD types prior to the SSW event in Figs. 3a and 3c, their differences in zonal-mean zonal wind anomaly are exhibited in Fig. 4. The differences in Figs. 4a and 4b are based on NCEP–NCAR, and those in Fig. 4c are based on MERRA. The data in Figs. 4a and 4b are based on a different period. However, all three panels of Fig. 4 share remarkable similarities regardless of the datasets and data period, showing negative values at high latitudes and positive differences at midlatitudes from the surface to the stratosphere.

To examine the effect of DS type on composite analysis studies, the differences in zonal-mean zonal wind anomaly between the DD type and DS+SS type

are shown in Fig. 5. This figure shows the differences between the displacement and split types as determined in previous studies; Fig. 5a can be compared with Fig. 7g of CP07, which uses the same dataset and analysis period. Figures 5a and 5b use different analysis periods, and the results differ significantly. This shows that the differences based on the two conventional types are dependent on the analysis period. The differences during the 1958–2002 period (Fig. 5a) are similar but weak compared with those in Fig. 4, and the negative differences over the polar region in Fig. 5a disappeared for the 1979–2014 period in Fig. 5b. This inconsistency between Figs. 5a and 5b have occurred because the DS type was included in the calculation. Characteristic features of the DS type in the 1958–2002 period seem to be different from those in the 1979–2014 period. In such a case, the DS type should be explicitly separated from other split-type events and should have its own classification.

### c. Comparisons with other studies

The central days and types of SSW events identified from NCEP–NCAR and MERRA data by using the method described in the previous section are listed in Table 1 (columns 2–5). The differences between the classification results from both datasets were negligible. To compare our classification with other well-known classifications, the results obtained from CJ11 are shown. It should be noted that CJ11 used the method of CP07. Subjective classification reported by CP07 is also included in Table 1 (column 8). The notations “D” and “S” used by CJ11 and CP07 correspond to our DD and combined DS+SS, respectively.

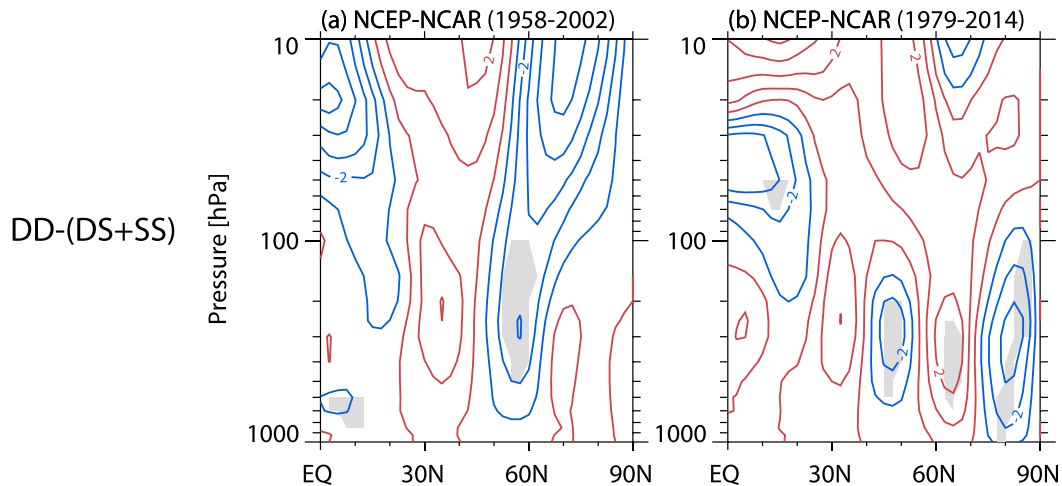


FIG. 5. As in Fig. 4, but for differences between DD and DS+SS types. The numbers of DD- and DS+SS-type events are 16 and 12 in (a) and 11 and 11 in (b), respectively.

According to our classification method, 20 DD, 10 DS, and 7 SS types were identified from NCEP–NCAR data (1957–2014), and 13, 7, and 5 were identified from MERRA data (1979–2014), respectively. The ratio of DD type to DS+SS type from NCEP–NCAR and MERRA data was about 1.18 and 1.08, respectively. The ratio is close to that reported by CP07 from 1957 to 2002, at 1.18. This shows that the results of our SSW-classification algorithm by wave amplitude are very similar to those resulting from the method of CP07.

The bold letters in Table 1 denote the SSW cases of different classifications from CJ11 (column 7). These four cases, represented in Table 1 as numbers 28 (15 December 1998), 29 (25 February 1999), 38 (21 January 2006), and 39 (24 February 2007), were investigated closely by comparison with the results of previous studies and analysis of the vortex shapes by GPH.

Concerning the case number 28, Kodera et al. (2016) demonstrated two separate vortices in GPH and the relative vorticity at 10 hPa by using reanalysis data. This case was also described by Mitchell et al. (2013) as a mixed event based on the distribution of potential vorticity. Number 29 was classified as DD type in our algorithm and was considered as a displacement type in Mitchell et al. (2013). However, in the reanalysis data, two separate vortices were identified after the central day. The wave-2 amplitude also increased gradually near the central day until the maximum value appeared after the central day (not shown). However, because the wave-2 amplitude was smaller than that of wave 1, this case was classified as DD type. Number 38 was classified as DD type by our criteria. Manney et al. (2008) considered it to be a wave-1 event based on the potential vorticity map calculated using satellite data, and Manney

et al. (2009) regarded it as displacement type. Number 39 is a rare case of SD type.

By using our simple method of wave amplitude calculation, we classified the SSW events as shown in Table 1. Of four cases of different classifications, only one case, number 29, was subtle; thus, our classification method appears to be effective for the other three cases.

We examined the frequency of each type for the five latitude belts of 10° width, shifting 5° from 45°–55° to 65°–75°N for the two reanalysis datasets. Table 2 shows the number of each SSW type according to the amplitude changes of wavenumbers 1 and 2 at the different latitudes. The ratio of DD to DS+SS types increases with latitude because the wave-2 amplitude decreases with latitude. For the belt of 55°–65°N, the ratio of DD type to DS+SS type was 1.18 for NCEP–NCAR data for 1957–2014, and 1.08 for MERRA data for

TABLE 2. Number of each SSW type occurring in different latitude belts based on NCEP–NCAR and MERRA data. Column 7 shows the ratio of DD to DS+SS types. The boldface text indicates the latitude band used for classification in this study.

Data	Latitude	Type				Ratio D/(DS+SS)
		DD	DS+SS	DS	SS	
NCEP–NCAR	45°–55°N	14	23	14	9	0.61
	50°–60°N	17	20	12	8	0.85
	<b>55°–65°N</b>	<b>20</b>	<b>17</b>	<b>10</b>	<b>7</b>	<b>1.18</b>
	60°–70°N	24	13	6	7	1.85
	65°–75°N	23	14	8	6	1.64
MERRA	45°–55°N	10	15	6	9	0.67
	50°–60°N	11	14	6	8	0.79
	<b>55°–65°N</b>	<b>13</b>	<b>12</b>	<b>7</b>	<b>5</b>	<b>1.08</b>
	60°–70°N	14	11	6	5	1.27
	65°–75°N	14	11	6	5	1.27

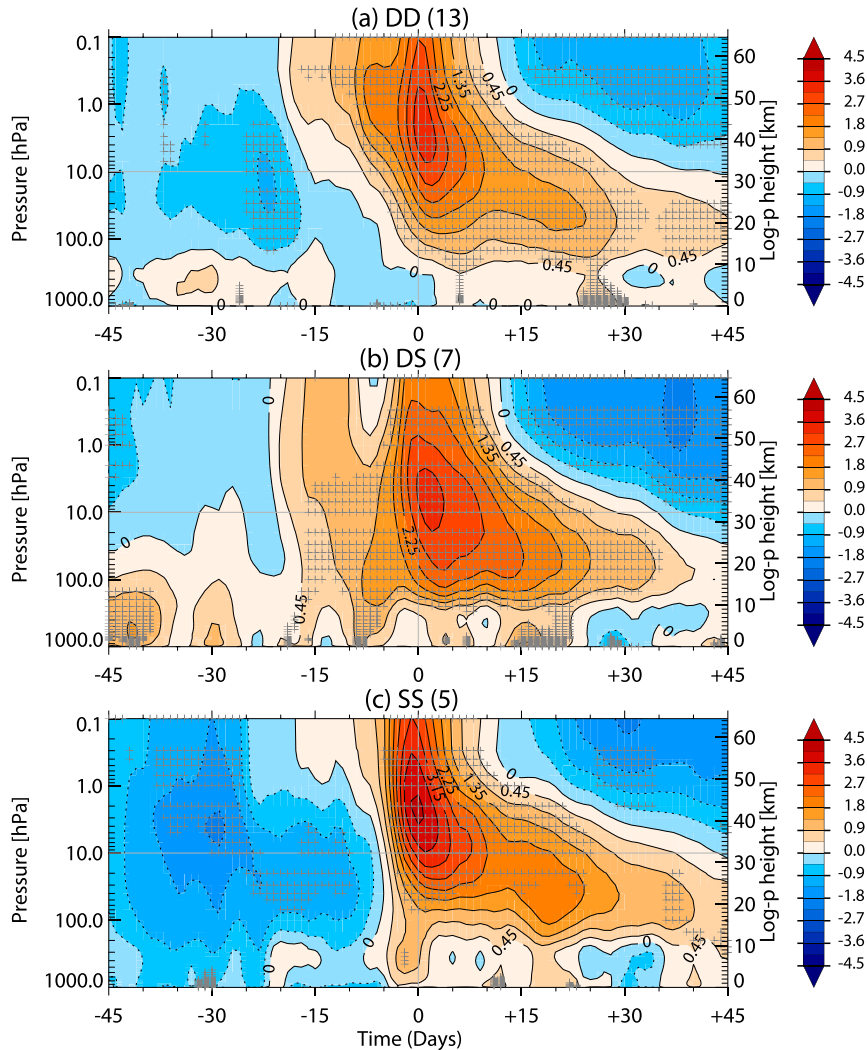


FIG. 6. PCH anomaly based on the MERRA GPH anomaly averaged over  $65^{\circ}$ – $90^{\circ}$ N for (a) 13 DD events, (b) 7 DS events, and (c) 5 SS events of SSW. Crosses indicate statistically significant regions at the 90% confidence level.

1979–2014, respectively; these results are similar to those reported by CP07.

We also tested the sensitivity of the classification type to the analysis period by changing the pre- and postevent periods from 10 to 15 days. Although the number of SS-type events remained the same, the number of DD- and DS-type events changed from 13 to 10 and from 7 to 10, respectively, owing to an increase in wave-2 activity after day +10. The identification and separation of the SS type from other types appears to be robust regardless of the analysis period.

#### d. Characteristic features of the three SSW types

To analyze the characteristic features of the three SSW types, composite means were obtained by using

both NCEP–NCAR and MERRA data. The results are insensitive to the dataset. Figure 6 shows a time–height cross section of the composite of the polar cap height (PCH) anomaly for each SSW type. Following Kim et al. (2014), the PCH anomaly was defined by the area-averaged GPH anomaly over the area north of  $65^{\circ}$ N and was normalized by its temporal standard deviation at each pressure level. The existence of a positive PCH anomaly corresponds to a weakened polar vortex.

Beginning on day  $-20$ , a positive PCH anomaly for the DD type (Fig. 6a) developed in the upper stratosphere and descended with time. The DS type (Fig. 6b) also showed the gradual descent of the positive PCH anomaly before the central day. The SS type (Fig. 6c) showed different characteristics from DD and DS types.

The negative PCH anomalies were dominant from the surface to the lower mesosphere until day  $-15$ . From around day  $-5$  the sudden descent of positive PCH anomalies was shown along the whole column.

Prior to the central day, ascent of the positive PCH anomaly from the troposphere to the stratosphere was observed in both DS and SS types beginning on days  $-10$  and  $-5$ , respectively; however, this phenomenon did not occur in the DD type. Afterward, the negative PCH anomaly descending from the upper to the middle stratosphere was larger for the DS and SS types compared with that for the DD type. Considering all the observations presented in Fig. 6, DS share more similarities with DD than SS before the central day.

Figure 7 shows the meridional cross sections of the MERRA zonal-mean zonal wind anomaly averaged over three periods for each type. During the prewarming period (Figs. 7a–c), the anomalies of zonal wind showed significant differences among the types, particularly between DS and SS, as expected by the aforementioned observations. In the stratosphere over the polar region, a negative anomaly dominated in the DS type, whereas in the SS type, the anomaly pattern formed a dipole structure centered at middle latitude throughout the entire stratosphere. To show the differences between DS and SS types more clearly, the anomaly of the combined DS+SS type is represented by a green contour in Figs. 7b and 7c. If we calculated the anomaly for the conventional split type, that anomaly would be close to this green contour. The green contour line at the polar middle stratosphere does not share similarities with either DS or SS anomalies. Thus, the separation of the conventional split types into DS and SS types has been validated.

Near the central day, three types showed similar anomalies with each other in the extratropical stratosphere; negative anomalies were also noted in the troposphere. In the postwarming period, all three types are characterized by the shifting of positive anomalies from the low-latitude middle stratosphere to the polar upper stratosphere and mesosphere. Among the three SSW periods shown in Fig. 7, the differences were most significant during the prewarming period, particularly between the DS and SS types; the differences in the later periods were smaller.

The meridional eddy heat flux represents the vertical component of the Eliassen–Palm flux and serves as an indicator of the vertical flux of wave activity from the troposphere into the stratosphere. To identify the vertical propagation of the planetary wave, the area-weighted meridional eddy heat flux anomaly is presented in Fig. 8.

For all types, the positive heat flux anomaly began to increase about 20 days before the central day. The

dominant wave component contributing to the total component differed among the types. In both DD and DS types, the wave-1 component accounted for most of the total component prior to the central day. The role of the wave-2 component was marginal throughout the period in the DD type, whereas it began to increase a few days before the central day in the DS type and dominated before the central day in the SS type. Moreover, the wave-1 component showed negative values after the central day in the SS and DS types.

In general, the DD and DS types showed similarities in total eddies and in the wave-1 component prior to the central day. We also calculated the composite mean of the meridional heat flux anomaly by using cases combining the DS and SS types. Although the results are not shown, they indicate that the wave-1 and wave-2 components are comparable and that the dominant wave components are not clearly distinguishable, which is in contrast to that shown in Figs. 8b and 8c.

One noteworthy point for the SS type is that a significant precursory positive heat flux anomaly caused by the wave-1 component occurred near day  $-30$ . Most of the SS-type SSW events occurred in the second half of winter; and minor warming events were observed prior to the occurrence. This precursor might capture the associated upsurge of wave activity. Although precursor was less clear in the DS type, it has been identified in the split type reported by CP07.

To investigate the possibility of tropospheric influence on the stratospheric waves in Fig. 8, the tropospheric anomaly fields for each type were examined. Figure 9 shows the zonal and vertical structure of the planetary wave anomaly averaged over the 45-day period prior to the central day. The vertical structure of the GPH anomaly field in the DS type (Fig. 9d) was similar to that in the DD type (Fig. 9a) and clearly differed from that in the SS type (Fig. 9g). In the DS and DD types, wave-1 anomalies were predominant (Figs. 9b and 9e). Their ridges and troughs shifted westward toward the upper level and were in phase with the winter climatological wave-1 pattern, which indicates that the planetary wave prior to the central day favors vertical propagation. The SS type exhibited a relatively weaker baroclinic structure, as was noted in previous studies (Martius et al. 2009; Matthewman et al. 2009). Because the wave-1 field for the SS type (Fig. 9h) exhibited negligible amplitude and was generally out of phase, showing large temporal variability, the contribution was relatively small. However, the wave-2 anomaly developed in phase with the climatological wave 2 (Fig. 9i).

Figure 10 shows the sea level pressure (SLP) anomaly averaged for the 45-day period before and after the central day. This figure can be compared with Fig. 1 of

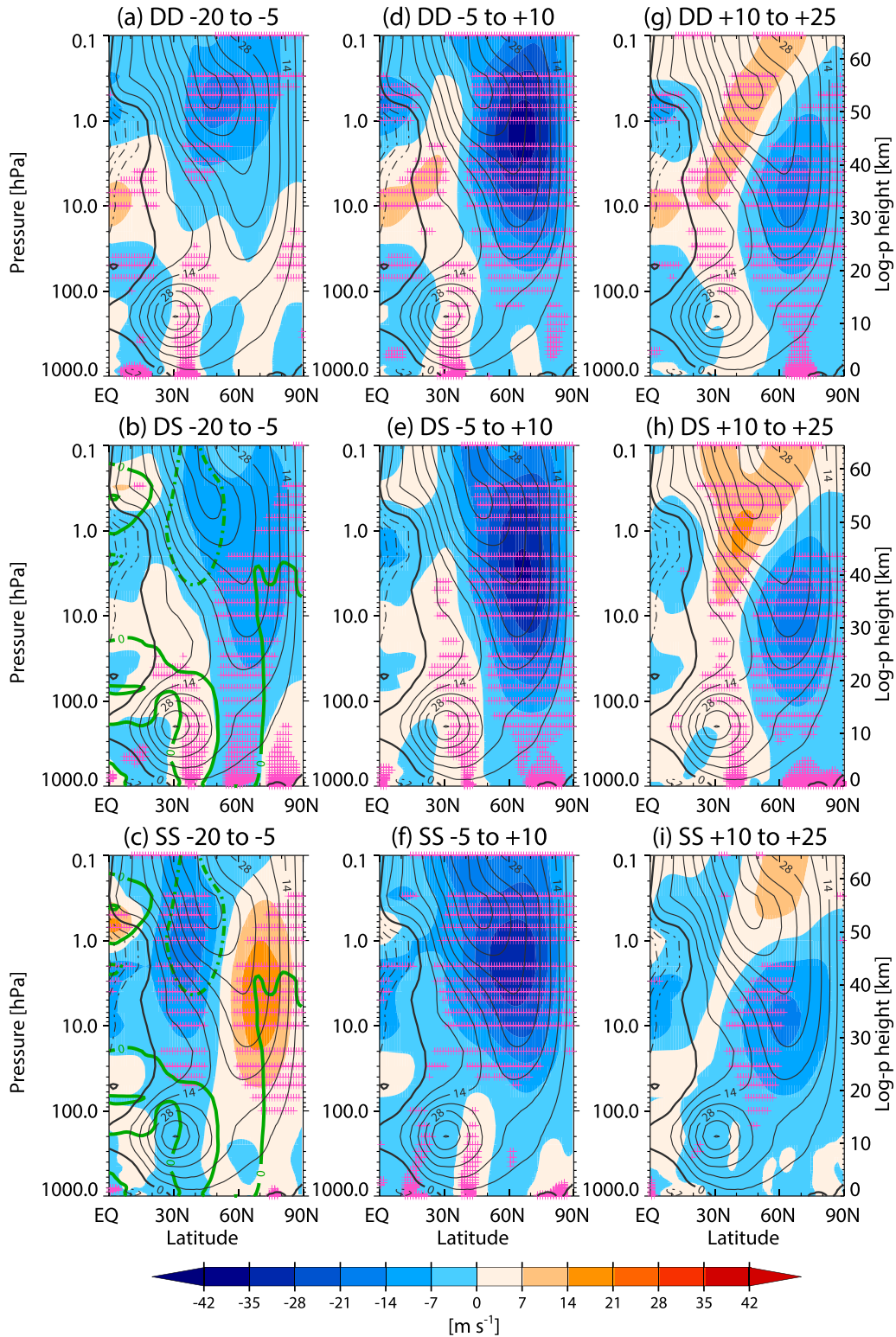


FIG. 7. Zonal-mean zonal wind anomaly (shading) and climatological December–February (DJF) mean and zonal-mean zonal wind (contours) based on MERRA data. The results are shown for (top) DD, (middle) DS, and (bottom) SS types, averaged (a)–(c) from days –20 to –5, (d)–(f) from days –5 to +10, and (g)–(i) from days +10 to +25. The thick solid and dashed–dotted contours denote zero and negative wind speeds, respectively. The contour interval is  $7 \text{ m s}^{-1}$ . Crosses indicate the statistically significant region at the 90% confidence level. The green contour (b) and (c) shows the wind anomaly using the combined DS+SS type.

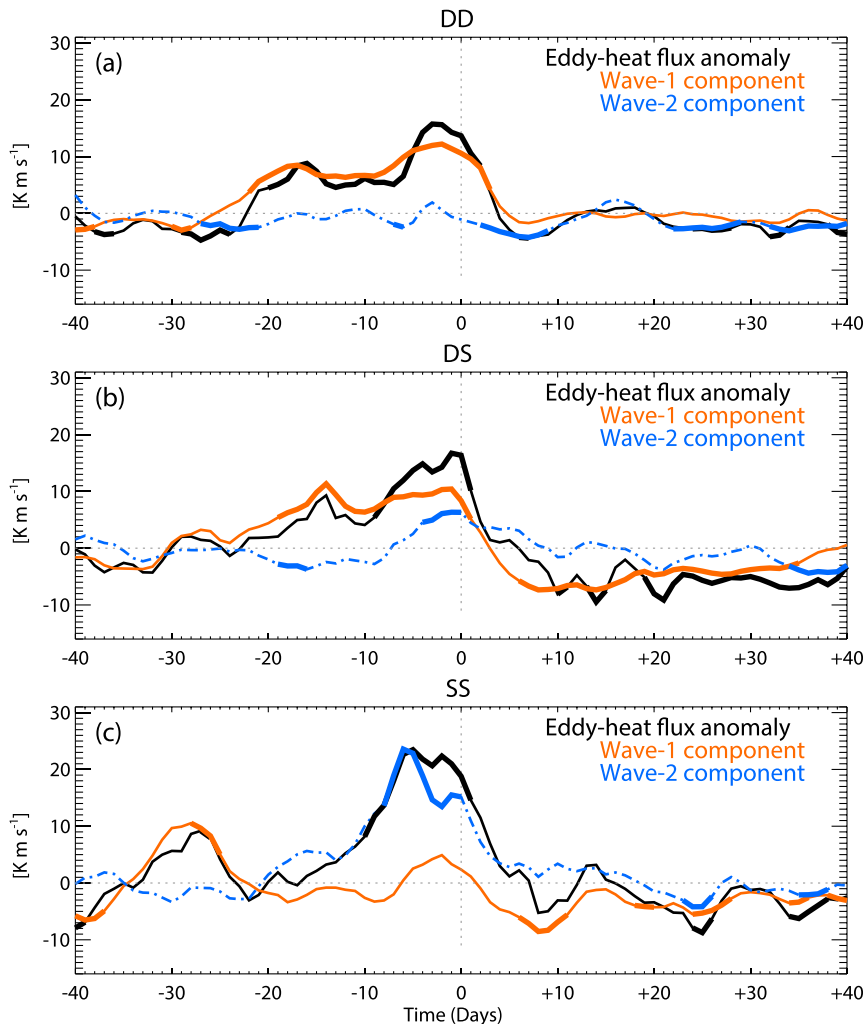


FIG. 8. Anomalies of meridional eddy heat flux averaged over  $45^{\circ}$ – $75^{\circ}$ N at 100 hPa based on NCEP–NCAR data for (a) DD, (b) DS, and (c) SS types. The black line denotes anomalies from the total eddies, and the orange and blue lines denote contributions by zonal waves 1 and 2, respectively. The thick solid part of each line indicates that the heat flux anomaly is significantly different from zero at the 90% confidence level.

CJ11, in which the categories of the displacement and split types were used. Although the location of the positive anomalies in Eurasia differs in DD and DS types (Figs. 10a and 10b), the SLP anomaly of both DD and DS types shows that positive anomalies in northwest of the Siberian high along with negative anomalies associated with the Aleutian low may have contributed to the formation of the wave-1 anomaly pattern in the stratosphere. On the contrary, for the SS type (Fig. 10c), the positive anomaly related to the Siberian high was weak, and a different positive anomaly was observed in the North Pacific region. This structure is favorable for wave-2 development (Martius et al. 2009; Nishii et al. 2011; CJ11). The spatial patterns in the SLP anomalies

prior to the SSW event are consistent with that shown in Fig. 9. During the postwarming period, the composite structures of the three types in the SLP anomaly (Figs. 10d–f) were qualitatively similar to that shown in CJ11.

#### 4. Model results

In the model results, SSW events occurred 103 times during the period of analysis. The frequency of SSW events per year, at 0.52, is smaller than that in the MERRA and NCEP–NCAR analyses, at 0.7 and 0.65, respectively. Among the 103 events of simulated SSW, 64 DD types, 31 DS types, and 8 SS types were

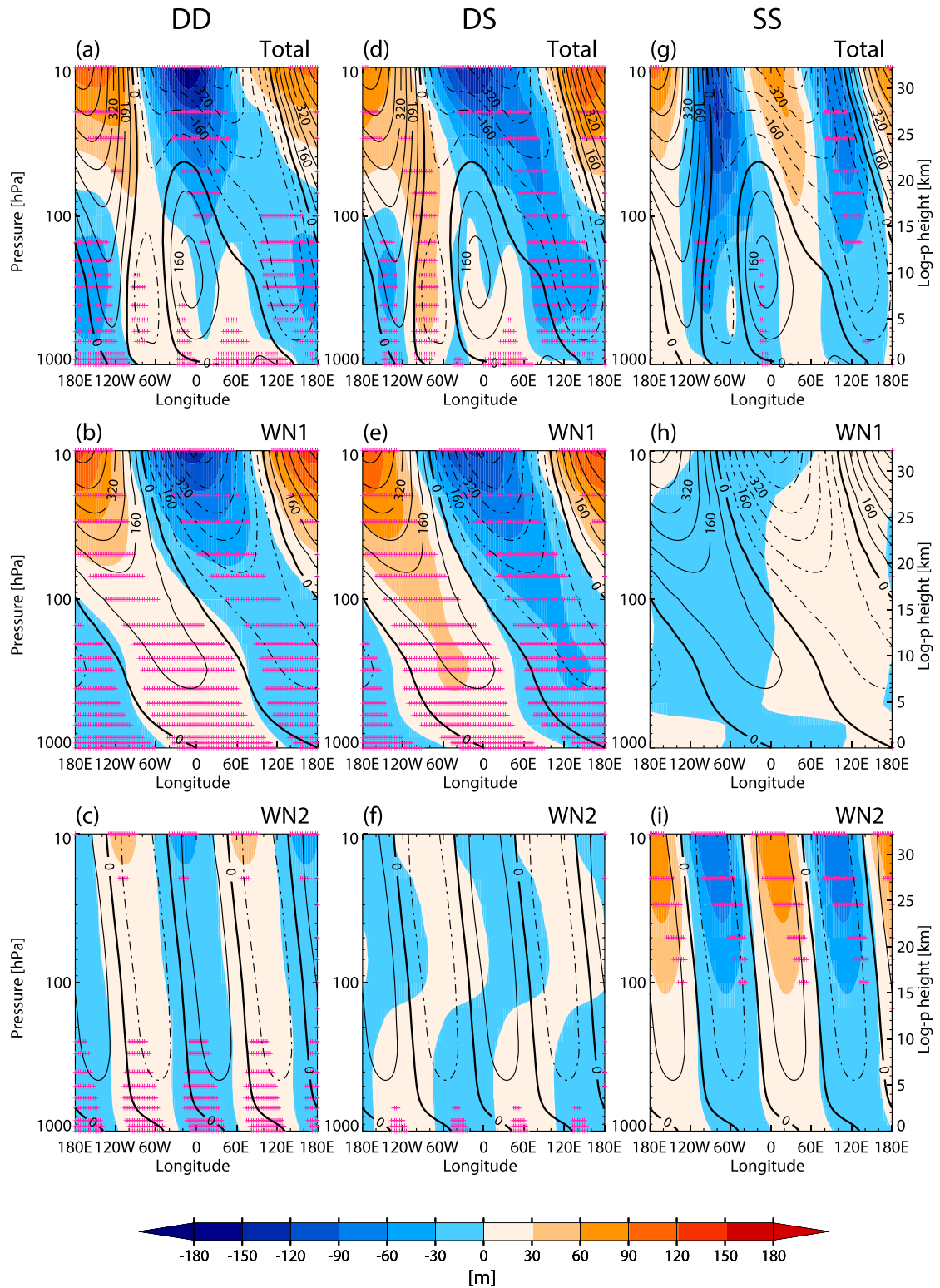


FIG. 9. GPH anomaly (shading) and climatological DJF mean values (contours) based on NCEP–NCAR data averaged from days  $-45$  to  $0$ . The GPH is averaged for latitude belts  $45^{\circ}$ – $75^{\circ}$ N. The results are shown for (a)–(c) DD, (d)–(f) DS, and (g)–(i) SS types. (top) The total anomaly, (middle) wave-1 anomaly, and (bottom) wave-2 anomaly. The thick solid and dashed–dotted contours denote zero and negative values, respectively. The contour interval is  $80$  m. Crosses indicate the statistically significant region at the  $90\%$  confidence level.

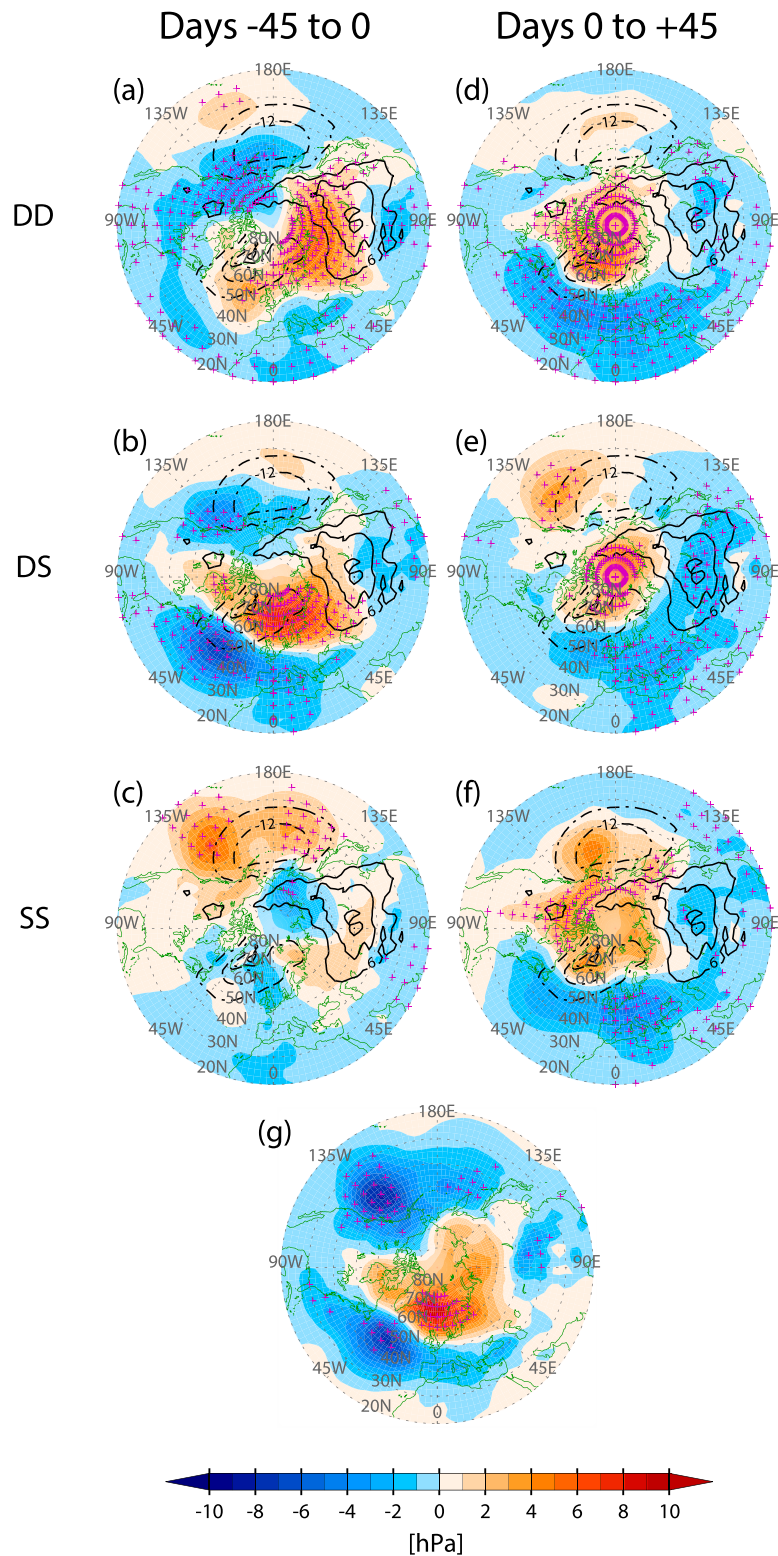


FIG. 10. SLP anomaly (shading) and zonal perturbation of DJF mean climatological values (contours) based on NCEP–NCAR data. Features averaged (left) from days  $-45$  to  $0$  and (right) from days  $0$  to  $+45$ . Shown are (a),(d) DD, (b),(e) DS, and (c),(f) SS types. (g) Difference between (b) and (c). The dashed-dotted contour denotes negative values. The contour interval is  $6$  hPa, and the zero contour is omitted. Crosses indicate statistically significant regions at the  $90\%$  confidence level.

TABLE 3. As in Table 2, but for WACCM results.

Data	Latitude	Type				Ratio
		DD	DS+SS	DS	SS	D/(DS+SS)
WACCM	45°–55°N	40	63	43	20	0.63
	50°–60°N	55	48	36	12	1.15
	<b>55°–65°N</b>	<b>64</b>	<b>39</b>	<b>31</b>	<b>8</b>	<b>1.64</b>
	60°–70°N	75	28	23	5	2.68
	65°–75°N	82	21	18	3	3.9

identified, which implies that displacement-type SSW events were produced twice as often as the split types combining DS and SS in the model. The occurrence of the modeled SS type was about one-fourth that of the DS type, whereas the DS and SS types occurred at comparable rates in the reanalysis data (Table 1). The high and low frequencies of the DD and SS types, respectively, imply that the model is more likely to produce a wave-1 pattern than a wave-2 pattern. Wave-2 amplified SSW is known to be associated with blocking in the Pacific basin region (Martius et al. 2009; Nishii et al. 2011; BC14); however, Pacific blocking was not easily reproduced in the model (de la Torre et al. 2012). Thus, the deficiency in the SS type appears to be consistent with the weak ability of the model in simulating Pacific blocking. The lack of the interannual variability in the boundary conditions of the model could also contribute to the low number of the SS-type SSWs.

The latitude belt selected for calculating the amplitude of the wave component is another factor determining the frequency of each type. We examined the frequencies for the five latitude belts of 10° width, shifting 5° from 45°–55° to 65°–75°N. Table 3 shows the frequency of each SSW type for the five latitude belts according to the model results. These model frequencies were more sensitive to the selected latitude belt than those of the reanalysis data (Table 2). As the selected latitude belt shifted to lower latitudes, the displacement types decreased, and the split types increased. For example, for the belt of 50°–60°N, the ratio of displacement type to split type was 1.15, which is similar to that from MERRA, at 1.08. The split-type increase in the model is attributed mostly to the increase in the DS type; the incidence of the SS type was still very low. We compared the composite means of the PCH anomaly from two different latitude belts, 50°–60° and 55°–65°N (not shown here). In contrast to the frequency change, the composite means of each type did not show significant differences in pattern depending on these two latitude belts.

To compare the model results with observations, all of the calculations performed by using the reanalysis data

were repeated by using the model results. The selected model analyses are shown in Figs. 11 and 12. Figure 11 shows a time–height cross section of the composite of the WACCM PCH anomaly for each SSW type. As indicated through a comparison with Fig. 6, the model appeared to effectively reproduce the major characteristic features of the observed SSWs.

The DD type (Fig. 11a) was generally similar to the DS type (Fig. 11b) and the observed DD type (Fig. 6a). Beginning on day around –30, positive PCH anomalies for the DD and DS types developed in the upper stratosphere and descended gradually with time. In the SS type from around day –5 sudden positive PCH anomalies were shown along the whole column. After the central day, the simulated DD and DS types showed that the stratospheric positive PCH anomaly descended to the troposphere with time. The negative PCH anomaly in the upper stratosphere also descended to the middle stratosphere. The largest anomaly appeared in the DS type (Fig. 11b), which agrees with the observations given in Fig. 6b. The model results and observations for the DS type differed, as evidenced by the lack of an ascending positive anomaly in the troposphere 10 days prior to the central day in the model results.

Figure 11c shows the negative PCH anomaly in the stratosphere from days –35 to –20 and the ascending positive PCH anomaly from the surface from days –10 to 0. The rapid shift in the sign of the PCH anomaly from negative to positive prior to the central day shown in the reanalysis was not clear in the model. The pattern of the ascent near –10 days in the troposphere is similar to that in the observed DS type shown in Fig. 6b.

For comparison with Fig. 7, latitude–altitude cross sections of the WACCM zonal-mean zonal wind anomaly averaged from day –20 to –5 are shown in Fig. 12. Similar to that discussed for Fig. 7, the zonal-mean wind patterns in this prewarming period exhibited relatively large differences among the types. The wind pattern in the DS type in Fig. 12b was more similar to that of the DD type (Fig. 12a) than the SS type (Fig. 12c); this result was also found in the observed wind fields shown in Fig. 7. In the SS type (Fig. 12c), although the observed wind anomaly in Fig. 7c showed a barotropic dipole pattern throughout the stratosphere, the zonal wind anomaly showed a more complex pattern.

## 5. Summary and discussion

To explain SSW events, major occurrences have been described in previous studies as either displacement or split type according to the shape of the polar vortex. The study by CP07 suggested an objective method of

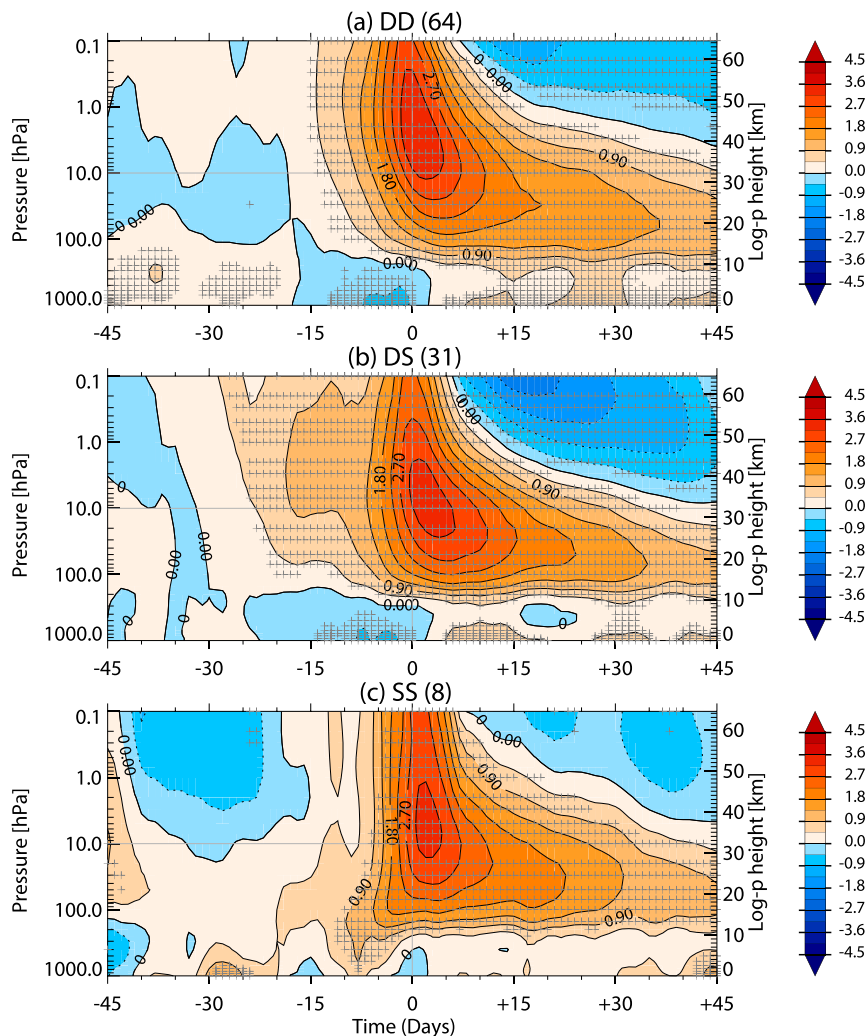


FIG. 11. As in Fig. 4, but for the PCH anomaly calculated by using the WACCM results for (a) 64 DD types, (b) 31 DS types, and (c) 8 SS types.

defining the SSW type by using the absolute vorticity on the isobaric surface; their method has been employed in recent studies (Martius et al. 2009; CJ11). Although this method appears to be applicable for separating the two types, it requires complex calculations and specifications of tunable parameters.

In this study, a more simple method was attempted for classifying SSW events by using the wave amplitude of planetary waves because zonal waves 1 and 2 develop during displacement-type and split-type SSW events, respectively. Following the commonly used definition of Butler et al. (2015), the central day of the SSW was specified by reversal of the zonal wind at 60°N and 10 hPa. Classification of the SSW events into two types of wave 1 and wave 2 is easily performed by comparing the wave amplitudes for 21 days from day -10 through

day +10, and the results are similar to those reported by CP07 for displacement and split types. Therefore, the classification by wave amplitude performed in this study is at least as reliable as that reported by CP07.

The classification method using daily amplitude has another advantage such that the temporal evolution is clearly revealed before and after the central day. Among the SSW events of the wave-2 type, the first group (Fig. 2a) exhibited the wave-2 shape only after the central day, whereas the second group (Fig. 2b) assumed this shape before and after the central day. Considering the significant differences between these two groups, we separated them into two types, DS and SS. The traditional displacement type is referred to as DD in our notation. The DD and DS types were relatively similar in the prewarming period.

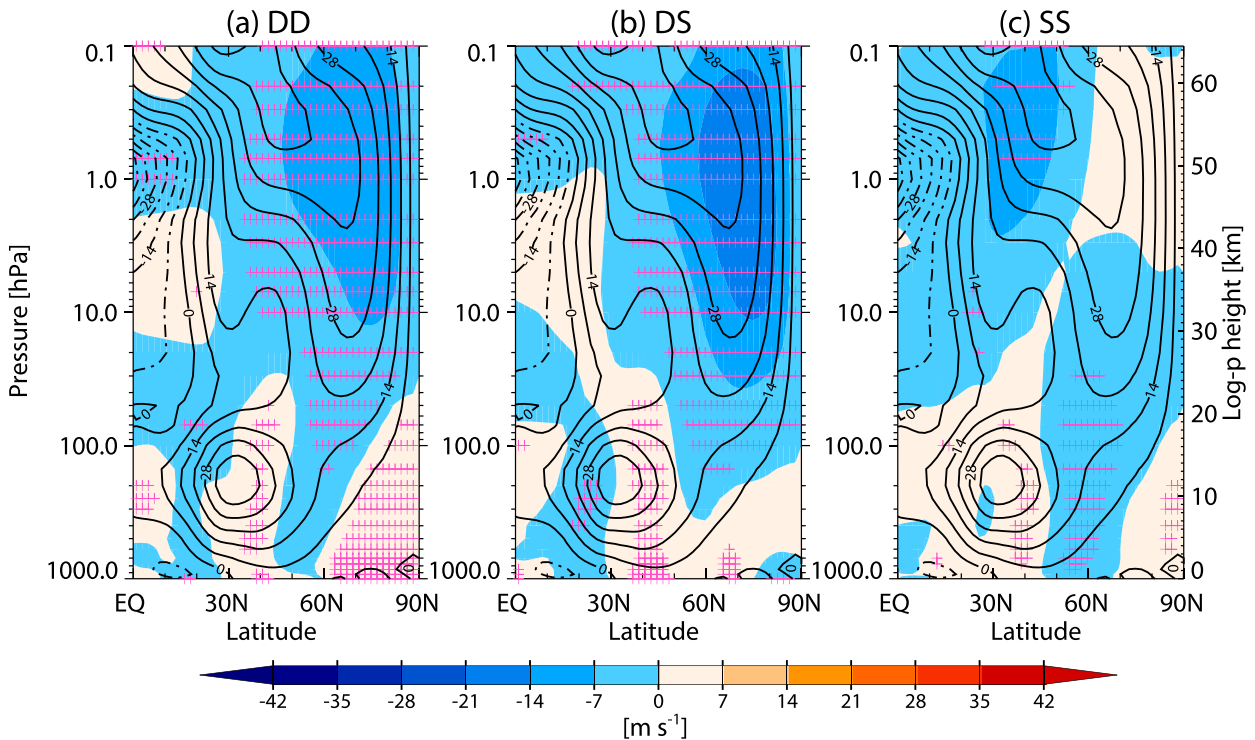


FIG. 12. As in Figs. 7a–c, but for WACCM data.

In the reanalysis data, the incidence number of DS and SS types was similar; however, different characteristics were exhibited including upward-propagating wave activity and a tropospheric height field prior to the central day of the SSW. The DS and SS types exhibited similar wave-2 behavior only close to the central day. Previous studies describing the split type, which is a combination of DS and SS types, appear to preferentially represent the features of the SS type (CP07; CJ11).

We also evaluated the ability of a state-of-art general circulation model in simulating SSW events of different types by using WACCM. In contrast to the classification results obtained by the reanalysis data, in which the DS+SS type occurred almost as often as the DD type, the split type in the WACCM occurred less frequently than the displacement type. Because the split type is simulated mostly in the form of the DS type in the model, and SS-type events are rare, the lower frequency of the split type can be attributed to the lack of SS-type simulations. Therefore, to obtain a more realistic simulation of stratospheric variability using WACCM, further research is needed to understand the reason for the significantly smaller number of SS events. Both tropospheric wave forcing and stratospheric internal variability of the model should be investigated carefully.

Although the occurrence frequency of the split type in the model tended to be sensitive to the changes in latitude belts used in the classification algorithm, the composite results were similar. The characteristic features reproduced by the model for DD and DS types were similar to those shown in the reanalysis data, whereas the observed and simulated SS types shared fewer similarities.

Classifying the SSW events into three types would also help in understanding the relevant dynamics associated with SSW and can contribute to improvement in the predictability of tropospheric weather change because SSW events are known to affect the stratosphere and surface weather (Baldwin and Dunkerton 1999, 2001; Thompson et al. 2002).

Although the DD and DS types appear to be similar, the mechanism of the wave 1 change to wave 2 for the DS type remains unknown and will be examined in future research.

*Acknowledgments.* The authors thank the three anonymous reviewers for their many helpful suggestions, which significantly improved the clarity and presentation of the paper. This work is funded by the Korea Polar Research Institute (KOPRI) Grant under project PE19130. WC is supported by the NRF (2018R1A2B6003197). BMK was supported by the Korea Meteorological Administration (2018-01014).

## REFERENCES

- Albers, J. R., and T. Birner, 2014: Vortex preconditioning due to planetary and gravity waves prior to stratospheric sudden warmings. *J. Atmos. Sci.*, **71**, 4028–4054, <https://doi.org/10.1175/JAS-D-14-0026.1>.
- Ayarzagüena, B., U. Langematz, and E. Serrano, 2011: Tropospheric forcing of the stratosphere: A comparative study of the two different major stratospheric warmings in 2009 and 2010. *J. Geophys. Res.*, **116**, D18114, <https://doi.org/10.1029/2010JD015023>.
- Baldwin, M. P., and T. J. Dunkerton, 1999: Propagation of the Arctic Oscillation from the stratosphere to the troposphere. *J. Geophys. Res.*, **104**, 30 937–30 946, <https://doi.org/10.1029/1999JD900445>.
- , and —, 2001: Stratospheric harbingers of anomalous weather regimes. *Science*, **294**, 581–584, <https://doi.org/10.1126/science.1063315>.
- Bancalá, S., K. Krüger, and M. Giorgetta, 2012: The preconditioning of major sudden stratospheric warmings. *J. Geophys. Res.*, **117**, D04101, <https://doi.org/10.1029/2011JD016769>.
- Barriopedro, D., and N. Calvo, 2014: On the relationship between ENSO, stratospheric sudden warmings, and blocking. *J. Climate*, **27**, 4704–4720, <https://doi.org/10.1175/JCLI-D-13-00770.1>.
- Butler, A. H., D. J. Seidel, S. C. Hardiman, N. Butchart, T. Birner, and A. Match, 2015: Defining sudden stratospheric warmings. *Bull. Amer. Meteor. Soc.*, **96**, 1913–1928, <https://doi.org/10.1175/BAMS-D-13-00173.1>.
- Charlton, A. J., and L. M. Polvani, 2007: A new look at stratospheric sudden warmings. Part I: Climatology and modeling benchmarks. *J. Climate*, **20**, 449–469, <https://doi.org/10.1175/JCLI3996.1>.
- Cohen, J., and J. Jones, 2011: Tropospheric precursors and stratospheric warmings. *J. Climate*, **24**, 6562–6572, <https://doi.org/10.1175/2011JCLI4160.1>; Corrigendum, 25, 1779–1790, <https://doi.org/10.1175/JCLI-D-11-00701.1>.
- Coy, L., S. Eckermann, K. Hoppel, and F. Sassi, 2011: Mesospheric precursors to the major stratospheric sudden warming of 2009: Validation and dynamical attribution using a ground-to-edge-of-space data assimilation system. *J. Adv. Model. Earth Syst.*, **3**, M10002, <https://doi.org/10.1029/2011MS000067>.
- de la Torre, L., R. R. Garcia, D. Barriopedro, and A. Chandran, 2012: Climatology and characteristics of stratospheric sudden warmings in the Whole Atmosphere Community Climate Model. *J. Geophys. Res.*, **117**, D04110, <https://doi.org/10.1029/2011JD016840>.
- Harada, A., A. Goto, H. Hasegawa, N. Fujikawa, H. Naoe, and T. Hirooka, 2010: A major stratospheric sudden warming event in January 2009. *J. Atmos. Sci.*, **67**, 2052–2069, <https://doi.org/10.1175/2009JAS3320.1>.
- Kalnay, E., and Coauthors, 1996: The NCEP/NCAR 40-Year Reanalysis Project. *Bull. Amer. Meteor. Soc.*, **77**, 437–471, [https://doi.org/10.1175/1520-0477\(1996\)077<0437:TNYRP>2.0.CO;2](https://doi.org/10.1175/1520-0477(1996)077<0437:TNYRP>2.0.CO;2).
- Kim, B.-M., S.-W. Son, S.-K. Min, J.-H. Jeong, S.-J. Kim, X. Zhang, T. Shim, and J.-H. Yoon, 2014: Weakening of the stratospheric polar vortex by Arctic sea-ice loss. *Nat. Commun.*, **5**, 4646, <https://doi.org/10.1038/ncomms5646>.
- Kodera, K., B. M. Funatsu, C. Claud, and N. Eguchi, 2015: The role of convective overshooting clouds in tropical stratosphere–troposphere dynamical coupling. *Atmos. Chem. Phys.*, **15**, 6767–6774, <https://doi.org/10.5194/acp-15-6767-2015>.
- , H. Mukougawa, P. Maury, M. Ueda, and C. Claud, 2016: Absorbing and reflecting sudden stratospheric warming events and their relationship with tropospheric circulation. *J. Geophys. Res. Atmos.*, **121**, 80–94, <https://doi.org/10.1002/2015JD023359>.
- Lawrence, Z. D., and G. L. Manney, 2018: Characterizing stratospheric polar vortex variability with computer vision techniques. *J. Geophys. Res. Atmos.*, **123**, 1510–1535, <https://doi.org/10.1002/2017JD027556>.
- Limpasuvan, V., J. H. Richter, Y. J. Orsolini, F. Stordal, and O.-K. Kvissel, 2012: The roles of planetary and gravity waves during a major stratospheric sudden warming as characterized in WACCM. *J. Atmos. Sol.-Terr. Phys.*, **78–79**, 84–98, <https://doi.org/10.1016/j.jastp.2011.03.004>.
- Manney, G. L., and Coauthors, 2008: The evolution of the stratosphere during the 2006 major warming: Satellite data and assimilated meteorological analyses. *J. Geophys. Res.*, **113**, D11115, <https://doi.org/10.1029/2007JD009097>.
- , and Coauthors, 2009: Aura Microwave Limb Sounder observations of dynamics and transport during the record-breaking 2009 Arctic stratospheric major warming. *Geophys. Res. Lett.*, **36**, L12815, <https://doi.org/10.1029/2009GL038586>.
- Marsh, D. R., M. J. Milis, D. E. Kinnison, J.-F. Lamarque, N. Calvo, and L. M. Polvani, 2013: Climate change from 1850 to 2005 simulated in CESM1 (WACCM). *J. Climate*, **26**, 7372–7391, <https://doi.org/10.1175/JCLI-D-12-00558.1>.
- Martius, O., L. M. Polvani, and H. C. Davies, 2009: Blocking precursors to stratospheric sudden warming events. *Geophys. Res. Lett.*, **36**, L14806, <https://doi.org/10.1029/2009GL038776>.
- Matthewman, N. J., J. G. Esler, A. J. Charlton-Perez, and L. M. Polvani, 2009: A new look at stratospheric sudden warmings. Part III: Polar vortex evolution and vertical structure. *J. Climate*, **22**, 1566–1585, <https://doi.org/10.1175/2008JCLI2365.1>.
- Mitchell, D. M., L. J. Gray, J. Anstey, M. P. Baldwin, and A. J. Charlton-Perez, 2013: The influence of stratospheric vortex displacements and splits on surface climate. *J. Climate*, **26**, 2668–2682, <https://doi.org/10.1175/JCLI-D-12-00030.1>.
- Neale, R. B., and Coauthors, 2012: Description of the NCAR Community Atmosphere Model (CAM 5.0). NCAR/TN-486+STR, 289 pp., [http://www.cesm.ucar.edu/models/cesm1.0/cam/docs/description/cam5\\_desc.pdf](http://www.cesm.ucar.edu/models/cesm1.0/cam/docs/description/cam5_desc.pdf).
- Nishii, K., H. Nakamura, and Y. J. Orsolini, 2011: Geographical dependence observed in blocking high influence on the stratospheric variability through enhancement and suppression of upward planetary-wave propagation. *J. Climate*, **24**, 6408–6423, <https://doi.org/10.1175/JCLI-D-10-05021.1>.
- O’Neill, A., 2003: Stratospheric sudden warmings. *Encyclopedia of Atmospheric Sciences*, J. R. Holton, J. A. Pyle, and J. A. Curry, Eds., Elsevier, 1342–1353.
- Rayner, N. A., D. E. Parker, E. B. Horton, C. K. Folland, L. V. Alexander, D. P. Rowell, E. C. Kent, and A. Kaplan, 2003: Global analyses of sea surface temperature, sea ice, and night marine air temperature since the late nineteenth century. *J. Geophys. Res.*, **108**, 4407, <https://doi.org/10.1029/2002JD002670>.
- Richter, J. H., F. Sassi, and R. R. Garcia, 2010: Toward a physically based gravity wave source parameterization in a general circulation model. *J. Atmos. Sci.*, **67**, 136–156, <https://doi.org/10.1175/2009JAS3112.1>.
- Rienecker, M. M., and Coauthors, 2011: MERRA: NASA’s Modern-Era Retrospective Analysis for Research and Applications.

- J. Climate*, **24**, 3624–3648, <https://doi.org/10.1175/JCLI-D-11-00015.1>.
- Smith, K. L., R. R. Neely, D. R. Marsh, and L. M. Polvani, 2014: The specified chemistry whole atmosphere community climate model (SC-WACCM). *J. Adv. Model. Earth Syst.*, **6**, 883–901, <https://doi.org/10.1002/2014MS000346>.
- Thompson, D. W. J., M. P. Baldwin, and J. M. Wallace, 2002: Stratospheric connection to Northern Hemisphere wintertime weather: Implications for predictions. *J. Climate*, **15**, 1421–1428, [https://doi.org/10.1175/1520-0442\(2002\)015<1421:SCTNHW>2.0.CO;2](https://doi.org/10.1175/1520-0442(2002)015<1421:SCTNHW>2.0.CO;2).
- Wang, R., Y. Tomikawa, T. Nakamura, K. Huang, S. Zhang, Y. Zhang, H. Yang, and H. Hu, 2016: A mechanism to explain the variations of tropopause and tropopause inversion layer in the Arctic region during a sudden stratospheric warming in 2009. *J. Geophys. Res. Atmos.*, **121**, 11 932–11 945, <https://doi.org/10.1002/2016JD024958>.
- Waugh, D. W., 1997: Elliptical diagnostics of stratospheric polar vortices. *Quart. J. Roy. Meteor. Soc.*, **123**, 1725–1748, <https://doi.org/10.1002/qj.49712354213>.
- Yoden, S., T. Yamaga, S. Pawson, and U. Langematz, 1999: A composite analysis of the stratospheric sudden warmings simulated in a perpetual January integration of the Berlin TSM GCM. *J. Meteor. Soc. Japan*, **77**, 431–445, [https://doi.org/10.2151/jmsj1965.77.2\\_431](https://doi.org/10.2151/jmsj1965.77.2_431).